International Research Journal of Innovations in Engineering and Technology (IRJIET)

ISSN (online): 2581-3048
Volume 9, Issue 5, pp 170-174, May-2025
https://doi.org/10.47001/IRJIET/2025.905021

Aerodynamic Load Analysis on Flapping Wings Using Unsteady Vortex-Lattice Method

[1]Khoiri Rozi, [2]*Ismoyo Haryanto, [3]Raihan Rafii' Herminasa

[1,2,3]Mechanical Engineering, Diponegoro University, Jl. Prof. H. Soedarto, SH, Tembalang, Semarang 50275, Indonesia
*Corresponding Author's E-mail: ismoyo2001@yahoo.de

***Abstract* - Aeroelastic studies of flapping wings on Micro Aerial Vehicle (MAV) that adopts bird or insect wing motion are very important because of their excellent maneuverability. Analysis in this simulation study with Unsteady Vortex-Lattice Methods (UVLM). The simulation results can be noted that in the downstroke motion, high vortex strength values produce significant lift force and vice versa in the upstroke. The greater flow deflection at high angles of attack and airfoil curvature that depends on the camber value produce pressure differences at the bottom and top of the wing. The lift force value affects the pitching moment value and induced drag value.**

Keywords: Aerodynamic Loads, FW-MAV, UVLM, Vortex Forces.

I. INTRODUCTION

The flapping wing motion in birds and insects has inspired many scientists to adopt it as a wing motion design in UAVs. Flapping wings have high aerodynamic efficiency at low Reynolds numbers by producing good lift and thrust and allowing for extraordinary maneuvers with rapid acceleration and deceleration [1]. This inspiration is applied in various fields, one of which is MAV which is used for various fields including civil and military [2]. The development of MAV design involving flapping wing motion is known as Flapping Wing Micro-Aerial Vehicle (FM-MAV). To maximize the performance of this FM-MAV, understanding wing kinematics, aerodynamics, and flexibility is the key to its success [3]. Understanding the unsteady aerodynamic loads generated by flapping wings is very important in the development of FM-MAV [4]. Known aerodynamic loads can improve system performance and become the basis for aeroelasticity analysis in the fluid-structure interaction of the wing [5][6]. However, flapping wings have very complex fluid-structure interactions due to flow unsteadiness. Wing flapping with frequency and amplitude will produce unstable flow patterns, vortices, and complex wing kinematics [7][8].

An efficient and effective analytical method is needed to understand the complexities of flapping wing aerodynamics. UVLM is a well-known aerodynamic model for calculating unsteady aerodynamic loads [9]. This method uses potential flow theory, neglects viscous effects at low Reynolds numbers, and provides results with inviscid and incompressible flows [10][11]. This method can also calculate aerodynamic loads in unsteady flows and handle the geometric complexity of flapping wing kinematics. This method allows modeling aerodynamic loads with fast computation time and high accuracy [13]. Python programming offers flexibility in implementing the numerical model. A simulation algorithm was developed by Urban (2021) to provide a suitable model and analysis [14].

II. METHODOLOGY

2.1 Unsteady Vortex-Lattice Method (UVLM)

UVLM is a development method of the Vortex-Lattice Method (VLM). This method can analyze the interaction of structures with fluids by observing the vortices formed on the surface of objects that change with each change in time. The surface of the object is divided into several lattices, each panel of which has a vortex formed and a control point. The vortex at the control point or panel has an induced velocity that changes because it is influenced by several factors. This method assumes incompressible, irrotational, and inviscid flow. In this method, the potential flow equation with zero normal flow conditions, namely no flow passing through the control points of the panels. To calculate the induced velocity value, it can be calculated using the Biot-Savart equation. The induced velocity is used to calculate the vortex strength value. The vortex strength value is used to calculate the force value on each panel using the Kutta-Joukowski theorem.

2.2 Model Test

This simulation uses Ptera software developed by Cameron Urban and has been validated [14][15]. Several parameter variations in this study such as airfoil profile, angle of attack (α), flap frequency (f), free stream velocity (U), air density (ρ), kinematic viscosity (ν) and sideslip angle (β) as in Table 1. The rectangular wing type is simulated with three flap steps, and the half span has 18 spanwise panels and 5 chordwise panels or has 90 panels. The flapping motion on the

International Research Journal of Innovations in Engineering and Technology (IRJIET)

ISSN (online): 2581-3048

Volume 9, Issue 5, pp 170-174, May-2025

https://doi.org/10.47001/IRJIET/2025.905021

wing utilizes fourth-order Fourier series data owned by Yeo et al., 2012.

Table 1: Measurement Parameters

NACA	0012; 2412
α (°)	15; 10; 5; 0; -5; -10; -15
f (Hz)	4.0; 4.5
$\rho\ (kg/m^3)$	1.204
$\nu\ (m^2/s)$	1515.06×10^{-6}
β (°)	0

2.3 Validation

The validation conducted by Urban (2021) is the reference in this study. The results of the validation conducted by Urbancan be seen in Figure 1.

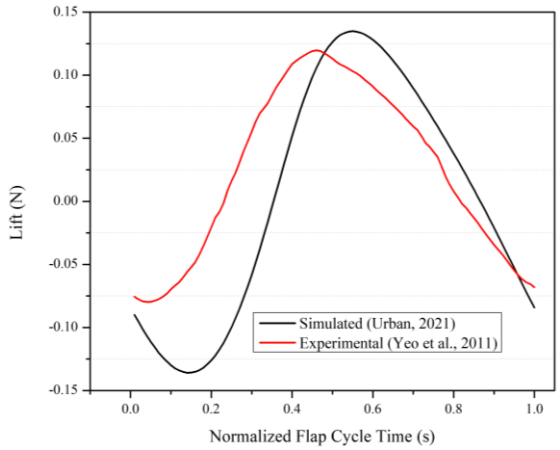

Figure 1: Validation of Simulation Result [13]

III. RESULTS AND DISCUSSIONS

3.1 Effects of the angle of attack

Figure 2 is the result of CL simulation on NACA 0012 with f = 4.5 Hz and U = 2.9 m/s. From the graph it can be seen that the amplitude of C_L increases with the increasing value of α for both pitched up and pitched down wings. The maximum lift value is produced during the downstroke and vice versa at maximum downward push. Wings with high lift produce small downward push values and vice versa. Pitched up wings produce higher lift values than pitched down wings. The highest positive C_L value is possessed by the wing with α = 15 °, which is C_L = 2.69 at θ = -8 ° and the highest negative C_L is possessed by the wing with α = -15 °, which is C_L = -2.50 at θ = 23.6 °. This happens because the greater the angle of attack, the greater the difference in pressure between the top and bottom of the wing. In the downstroke phase, the airflow velocity above the strong wing increases and the pressure under the wing increases, resulting in high lift. Conversely, in the upstroke phase, the flow velocity decreases and the pressure above the wing increases, resulting in higher downward push.

The simulation results of C_{PM} for the NACA 0012 profile are shown in Figure 3. From this plot, it is found that the C_{PM} distribution has a periodic pattern. The positive C_{PM} value is influenced by the downward push force value which indicates that its peak value is produced during the upstroke phase and vice versa. In addition, the highest positive C_{PM} value is influenced by the position of the wing pressure center which is behind the center of gravity (CG). The highest positive C_{PM} peak value is possessed by the object wing with α = -15° which has C_{PM} = 1.17 at θ = 25.4° and the lowest positive C_{PM} peak value is possessed by the object wing with α = 15° which has C_{PM} = 0.27 at θ = 25.8°. Meanwhile, the highest negative C_{PM} peak value is possessed by the object wing with α=15° which has C_{PM}=-0.93 with θ=-18° and the lowest at α=-15°, namely C_{PM}=-0.26 with θ=-17°.

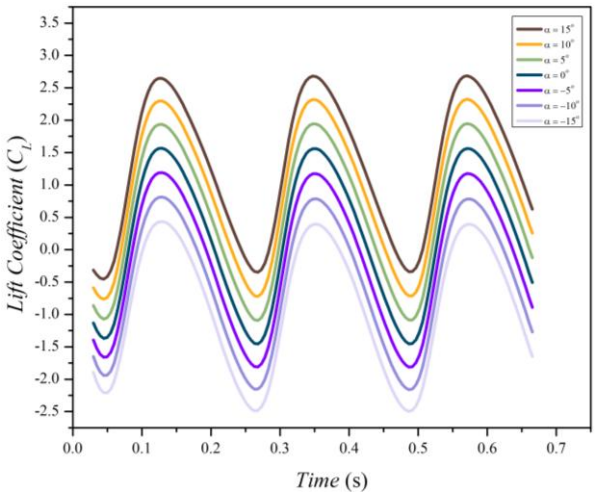

Figure 2: Distribution of $C_L$as a funtion of time at $f = 4.5$ Hz with NACA 0012 and U = 2.9 m/s

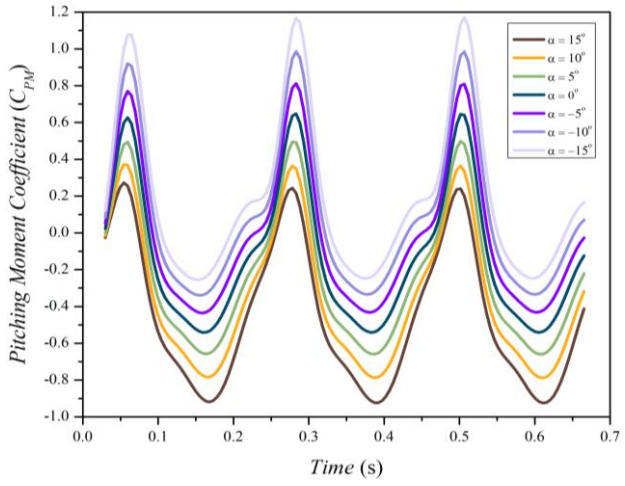

Figure 3: Distribution of C_{PM}at $f = 4.5$ Hz and U = 2.9 m/s for NACA 0012

International Research Journal of Innovations in Engineering and Technology (IRJIET)

ISSN (online): 2581-3048

Volume 9, Issue 5, pp 170-174, May-2025

https://doi.org/10.47001/IRJIET/2025.905021

Simulation results of the induced drag for the NACA 0012 is plotted in Figure 4. From this plot it can be shown that the greater the angle of attack on the wing, the greater the induced drag. The smallest induced drag occurs at the base degree. The pitched up wing has a positive peak C_{DI} value during the upstroke and negative during the downstroke and vice versa. In the upstroke phase, induced drag increases due to unstable wingtip vortices, while the opposite occurs in the pitched down wing. The highest positive peak C_{DI} value is possessed by the wing with α = -15°, namely C_{DI} = 0.37 with θ = 24.3°. The lowest C_{DI} value occurs at α = 0°, namely C_{DI} = 0.08 with θ = -17.5°. In addition, it is shown that the highest negative C_{DI} peak value occurs at α=-15°, namely C_{DI}=-0.56 with θ=7.8° and the lowest at α=0°, namely C_{DI}=-0.39 with θ=-17.5°.

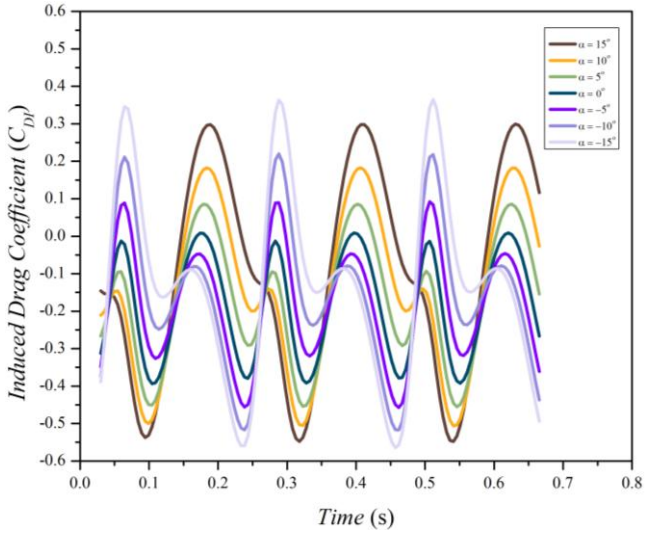

Figure 4: Distribution of C_{DI} at $f = 4.5$ Hz and U = 2.9 m/s for NACA 0012

3.2 Influences of the flapping frequency on the C_L

The simulation results of C_L values for NACA 2412 with f=4.0; and 4.5 Hz are presented in Figure 5 and Figure 6. At the flapping frequency f=4.0 the highest C_L peak value occurs at α=15°, namely C_L=2.52 at θ=-7.2° and the lowest C_L peak value at α=-15°, namely C_L=0.28 at θ=-8.8°. The highest negative C_L peak value is possessed by the wing at α=-15°, namely C_L=-2.29 and θ=23.2° and the lowest negative C_L peak value is possessed by the wing at α=15°, namely C_L=-0.25 at θ=22.8°. Shown in Figure 6, there is an increase in the amplitude of the C_L value and also the value of the flap angle change for each time change caused by the increase in flap frequency. According to this graph, the highest peak C_L value in this plot is owned by the object wing with α=15° which has C_L=2.69 when θ=-8° and the lowest peak $C_L$at α=-15° which has C_L=0.44 when θ=-9.3°.

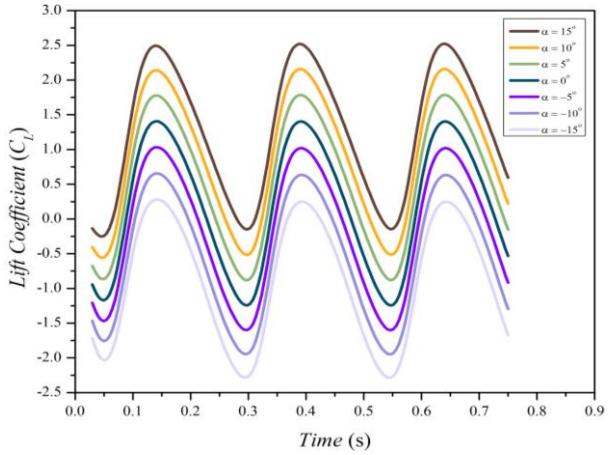

Figure 5: Characteristic of C_L at $f = 4.0$ Hz and U = 2.9 m/s for NACA 2412

Meanwhile, the highest negative C_L value is produced by the object wing with α=-15° which has C_L=-2.50 when θ=23.6° and the smallest negative peak C_L value is owned by the object wing with α=15° which has C_L=-0.45 when θ=24.4°. This can happen when the wing flaps, the air around the wing will experience acceleration. The higher the flapping frequency, the higher the flow acceleration value. The higher the air acceleration value, the higher the force acting on the wing.

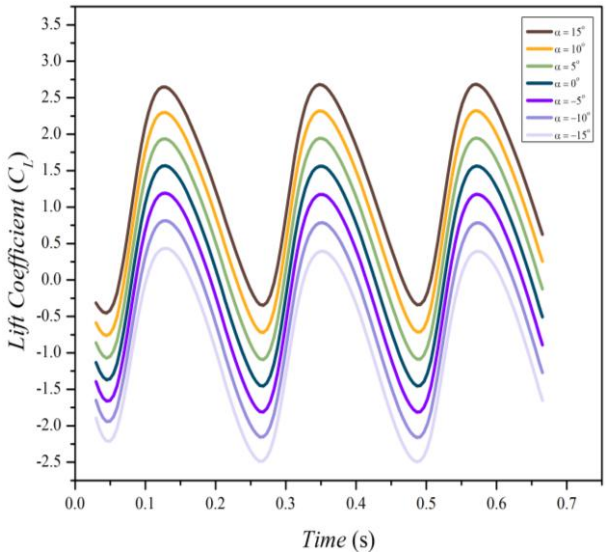

Figure 6: Characteristic of $C_L$at $f = 4.5$ Hz and U = 2.9 m/s for NACA 2412

3.3 Influences of the flapping frequency on the C_{PM}

Figure 7 shows the results of the C_{PM} simulation against time at f = 4.0 Hz. From this plot, it can be seen that the highest positive C_{PM} peak value is owned by the object wing with α = -15 ° which has C_{PM} = 0.99 at θ = 25.6 ° and the lowest positive C_{PM} peak value is owned by the object wing with α = 15 ° which has C_{PM} = 0.19 at θ = 25.8 °. For the highest negative C_{PM} peak value itself, it is owned by the

International Research Journal of Innovations in Engineering and Technology (IRJIET)

ISSN (online): 2581-3048

Volume 9, Issue 5, pp 170-174, May-2025

https://doi.org/10.47001/IRJIET/2025.905021

object wing with α = 15 ° which has C_{PM} = -0.82 with θ = -18 ° and the lowest is owned by the object wing with α = -15 ° which has C_{PM} = -0.2 with θ = -16.3°.

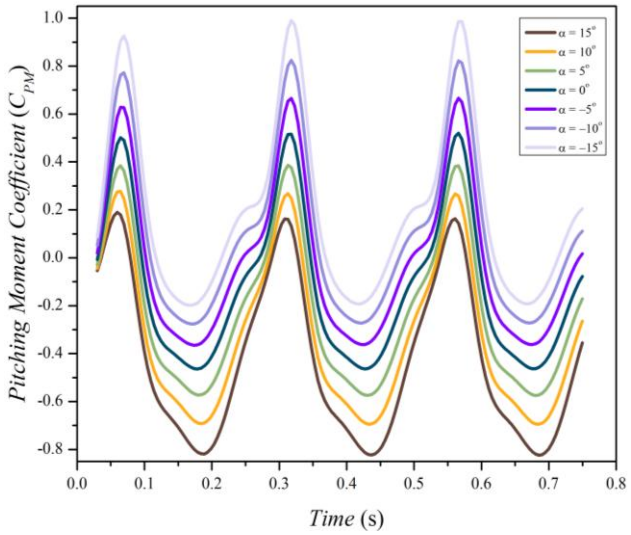

Figure 7: Characteristic of C_{PM} at $f = 4.0$ Hz and U = 2.9 m/s for NACA 2412

Figure 8 shows the C_{PM} value at f = 4.5 Hz. It is shown that the highest positive C_{PM} peak value is possessed by the object wing with α=-15° which has C_{PM}=1.17 at θ=25.4° and the lowest positive C_{PM} peak value is possessed by the object wing with α=15° which has C_{PM}=0.27 at θ=25.8°. Meanwhile, the highest negative C_{PM} peak value is possessed by the object wing with α=15° which has C_{PM}=-0.93 with θ=-18° and the lowest is possessed by the object wing with α=-15° which has C_{PM}=-0.26 with θ=-17°. As previously explained, the pitching moment value is greatly influenced by the lift force value. Therefore, the amplitude of the pitching moment value will increase along with the increasing amplitude of the lift force value due to the increasing frequency of wing flaps.

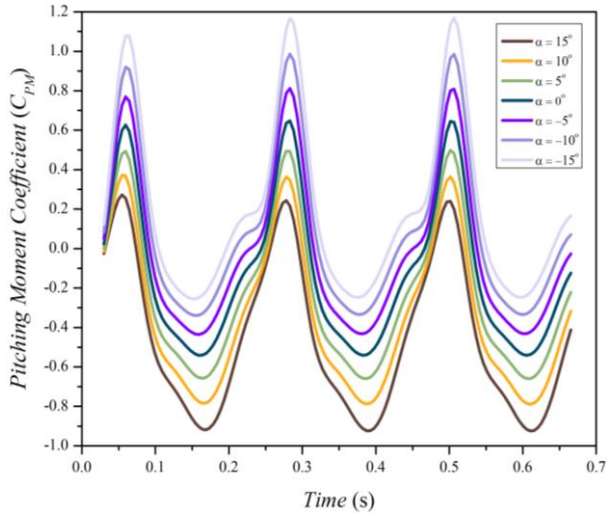

Figure 8: Characteristic of C_{PM} at $f = 4.5$ Hz and U = 2.9 m/s for NACA 2412

3.4 Influences of the flapping frequency on the C_{DI}

Figure 9 shows the simulation results of the C_{DI} as a function of time at f = 4.0 Hz. From the plot in this figure, it can be seen that the highest C_{DI} value is produced by the object wing with α=-15° which has C_{DI}=0.31 at θ=24.1° and the smallest peak C_{DI} value is produced by the object wing with α=0° which has C_{DI}=0.02 at θ=-17.6°. Meanwhile, the highest negative C_{DI} value is produced by the object wing with α=-15° which has C_{DI}=-0.46 at θ=9.2° and the smallest negative peak C_{DI} value is produced by the object wing with α=0° which has C_{DI}=-0.32 at θ=3.4°.

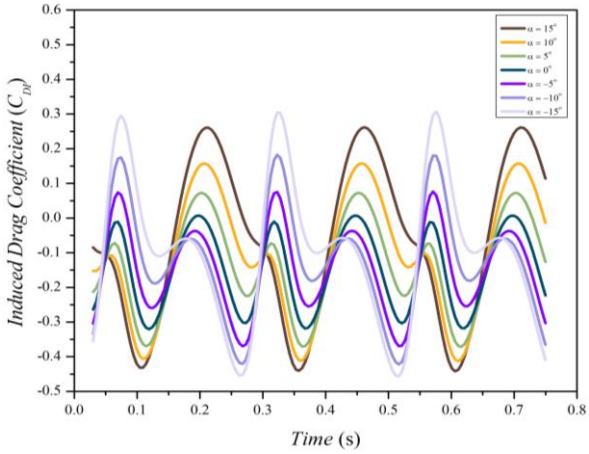

Figure 9: Characteristic of C_{DI} as a fuction of time at $f = 4.0$ Hz and U = 2.9 m/s for NACA 2412

The C_{DI} value increases with increasing flapping frequency to f=4.5 Hz as plotted in Figure 10. From this plot, it shows that the highest positive C_{DI} peak value is owned by the object wing with α=-15° which has C_{DI}=0.37 with θ=24.3° and the lowest is owned by the object wing with α=0° which has C_{DI}=0.08 with θ=-17.5°. In addition, it is shown that the highest negative C_{DI} peak value is owned by the object wing with α=-15° which has C_{DI}=-0.56 with θ=7.8° and the lowest at α=0° which is C_{DI}=-0.39 with θ=-17.5°.

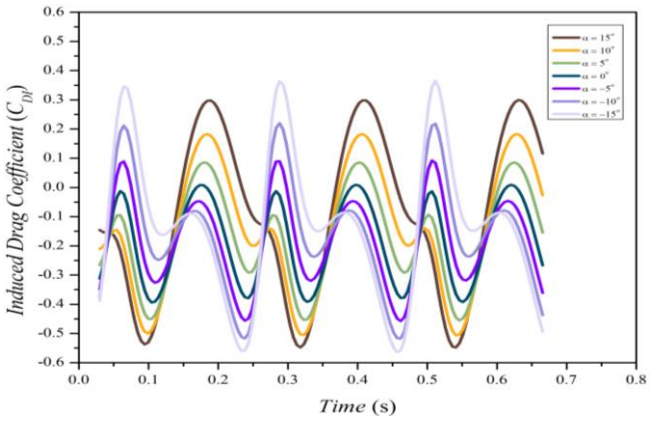

Figure 10: Characteristic of C_{DI} at $f = 4.5$ Hz and U = 2.9 m/s for NACA 2412

ISSN (online): 2581-3048
Volume 9, Issue 5, pp 170-174, May-2025
https://doi.org/10.47001/IRJIET/2025.905021

IV. CONCLUSION

Based on the simulation, the following important results can be summarized: The unsteady vortex-lattice method is used to analyze the interaction of fluid and solid objects to determine the aerodynamic loads. Increasing the angle of attack causes an increase in lift force and downward push due to the pressure difference on the wing. The position of the center of pressure relative to the center of gravity affects the pitching moment and induced drag depending on the downward push. Wing flapping at a higher frequency increases the applied force. Airfoils with camber produce more lift than symmetrical airfoils. Increasing the flow velocity decreases the vortex strength and the resulting force. The highest pressure is at the leading edge and decreases along the chord, with a non-uniform distribution along the spanwise due to wing tip vortex disturbances.

REFERENCES

[1] Liu, K., Ronch, A. Da, Li, D. and Xiang, J. 2015. Modeling of Unsteady Aerodynamics for a Flapping wing. *IFAC-PapersOnLine*. 48, 28 (2015), 404–408.

[2] Shyy, W., Berg, M. and Ljungqvist, D. 1999. Flapping and flexible wings for biological and micro air vehicles. *Progress in Aerospace Sciences*. 35, 5 (1999), 455–505.

[3] Shyy, W., Aono, H., Chimakurthi, S.K., Trizila, P., Kang, C.-K., Cesnik, C.E.S. and Liu, H. 2010. Recent Progress in Flapping Wing Aerodynamics and Aeroelasticity. *Progress in Aerospace Sciences*. 46, 7 (2010), 284–327.

[4] Au, L.T.K., Phan, H.V. and Park, H.C. 2017. Comparison of Aerodynamic Forces and Moments Calculated by Three-dimensional Unsteady Blade Element Theory and Computational Fluid Dynamics. *Journal of Bionic Engineering*. 14, 4 (2017), 746–758.

[5] Ruiz, C., Acosta, J. and Ollero, A. 2022. Aerodynamic reduced-order Volterra model of an ornithopter under high-amplitude flapping. *Aerospace Science and Technology*. 121, (2022), 107331.

[6] Beker, C., Turgut, A.E., Arikan, K.B. and Kurtulus, D.F. 2020. Aeroelastic Analysis of a Flapping Blow Fly Wing. *International Journal of Aviation Science and Technology*. 1, 1 (2020), 14–21.

[7] Li, L., Xu, J., Gao, Y., Yang, J., Bai, F. and Wang, Y. 2022. Unsteady aerodynamic characteristics of a bionic flapping wing in three-dimensional composite motion. *AIP Advances*. 12, 1 (2022).

[8] Kang, C.-K., Aono, H., Cesnik, C.E.S. and Shyy, W. 2011. Effects of Flexibility on the Aerodynamic Performance of Flapping Wings. *Journal of Fluid Mechanics*. 689, (2011), 32–74.

[9] Simpson, R.J.S., Palacios, R. and Murua, J. 2013. Induced-drag calculations in the unsteady vortex lattice method. *AIAA Journal*. 51, 7 (2013), 1775–1779.

[10] Murua, J., Palacios, R. and Graham, J.M.R. 2012. Applications of the unsteady vortex-lattice method in aircraft aeroelasticity and flight dynamics. *Progress in Aerospace Sciences*. 55, (2012), 46–72.

[11] Roccia, B.A., Preidikman, S., Massa, J.C. and Mook, D.T. 2013. Modified unsteady vortex-lattice method to study flapping wings in hover flight. *AIAA Journal*. 51, 11 (2013), 2628–2642.

[12] Souza, E. de, Silva, R.G.A. da and Cesnik, C.E.S. 2014. an Object-Oriented Unsteady Vortex Lattice Method for Aeroelastic Analyses of Highly Flexible Wings. *Proceedings of 10th World Congress on Computational Mechanics*. 1, (2014), 2064–2083.

[13] Urban, C. 2021. Validation and Optimization of Ptera Software: An Open-Source Unsteady Simulator for Flapping Wings. (2021).

[14] Yeo, D., Atkins, E.M. and Shyy, W. 2011. Experimental and analytical pressure characterization of a rigid flapping wing for ornithopter development. *AIAA Atmospheric Flight Mechanics Conference 2011*. August (2011), 1–18.

[15] Ptera Software: 2020. https://github.com/camUrban/PteraSoftware.

Citation of this Article:

Khoiri Rozi, Ismoyo Haryanto, & Raihan Rafii' Herminasa. (2025). Aerodynamic Load Analysis on Flapping Wings Using Unsteady Vortex-Lattice Method. *International Research Journal of Innovations in Engineering and Technology - IRJIET*, 9(5), 170-174. Article DOI https://doi.org/10.47001/IRJIET/2025.905021

****

